8A.3 Thermodynamic and Kinematic Analysis of a Tornadic Supercell using High Resolution In Situ Data from Texas Tech StickNet Instrument Systems

Bradley R. Charboneau* and Christopher C. Weiss
Texas Tech University, Lubbock, TX

1. INTRODUCTION

In May and June of 2009 and 2010, over 100 scientists, students and volunteers embarked on the largest tornado research project in history: The Verification of the Origins of Rotation in Tornadoes EXperiment 2 (VORTEX2). This scientific armada was equipped with the latest technologies in the field - including several mobile Doppler radars, surface observation platforms, radiosondes, and disdrometers - and aimed to quantify the environment within and surrounding tornadic supercells to an unprecedented degree. Texas Tech played an integral role in this project by deploying a total of 650 StickNet platforms, designed specifically for safely measuring crucial thermodynamic and kinematic variables within hostile regions of storms.

Of critical importance to the numerous scientific objectives sought out in VORTEX2 is the observation and analysis of baroclinity within tornadic and non-tornadic supercells. Numerous studies have revealed that streamwise vorticity generation due to baroclinity is critical to low-level mesocyclogenesis and tornadogenesis. However, recent observational studies have shown that supercells with relatively small thermodynamic deficits between the inflow and both the rear flank and forward flank environments are more likely to produce longer lived and violent tornadoes than those with large deficits (Markowski et al. 2002; Shabbot et al. 2006; Grzych et al. 2007). Other studies have shown that individual storm scale environments exhibit substantial temporal and spatial variability, thus making it difficult to adequately diagnose the state of a storm with limited observations (Hirth 2008). Although much has been learned from these studies, scientists' understanding of baroclinity within supercells remains largely incomplete, and thus a clear relationship to tornadogenesis remains elusive.

In this presentation, StickNet data will be used to analyze the thermodynamic and kinematic properties of the forward and rear flanks of the June 5th, 2009 LaGrange, WY supercell. Time-to-space conversion methods will be used to analyze the bulk spatial thermodynamic characteristics of the storm, while individual traces of data will be used to examine small-scale features and assess the heterogeneity of the storm scale environment.

2. DATA COLLECTION AND ANALYSIS

a. StickNet Platforms

Beginning in 2005, students and faculty from Texas Tech's Wind Engineering and Atmospheric Science programs developed the first "StickNet" probe – a durable, rapidly deployable meteorological observation station designed specifically for the safe collection of high-resolution data within hostile storm environments. Since the initial construction of two prototypes, the fleet has grown to 24 fully functioning probes, and has successfully sampled numerous severe weather phenomena

Two versions of the probes exist in the current fleet. "A" probes utilize analog instruments and are capable of collecting 1, 5 and 10 Hz measurements of wind speed, wind direction, barometric pressure, temperature, and relative humidity. "B" probes utilize a Vaisala all-in-one instrument to make those same measurements with the addition of hail and rainfall, but are restricted to a 1 Hz sampling frequency. Both versions utilize a GPS receiver and a flux compass to calculate the location and the orientation of the probe (Weiss and Schroeder 2008). At the start of the project, there were approximately 14 A probes and 10 B probes; however, a few B probes were converted to A probes due to hail damage to the Vaisala instruments in the 2010 phase of VORTEX2.

*Corresponding author address: Bradley R. Charboneau, Texas Tech University, Atmospheric Science Group, Department of Geosciences, Lubbock, TX, 79409; email: brad.charboneau@ttu.edu

b. Deployment Strategy

Before operations on a given day, the StickNet probes were divided into four vehicles that each had a specific task. Seven probes were placed in each of two trailers, while five probes were fastened to custom-built racks in the bed of two standard pickup trucks. Each trailer was paired with a pickup truck, and these pairs each were responsible for an individual array of probes. Once VORTEX2 declared a viable target storm for operations, the StickNet field coordinator established a deployment strategy that was relayed to each deployment team.

Assuming a reasonable storm motion and speed, the ideal strategy was to deploy two independent north-to-south arrays, each of which was spaced as close to each other as the available road network and storm motion allowed. In each array, seven probes were dedicated to a coarse spacing of approximately 2-5 km, while five probes were dedicated to a nested fine scale array with spacing of 1-2 km. The coarse array was responsible for obtaining a broad sample of all regions of the target storm, while the fine scale array was positioned with the intention of taking high-resolution measurements centered on the low-level mesocyclone. This strategy allowed the field coordinator to cast an initial wide "net" with the coarse array early in the deployment (~60-75 minutes prior to mesocyclone intercept), and then later deploy the fine scale array when the location of the mesocyclone array-crossing could be reliably ascertained (~30-45 minutes prior to intercept). In practice, erratic storm motions and poor road networks often made this strategy nearly impossible to strictly adhere to. However, the deployment strategy was flexible enough to be successfully adapted to many situations.

c. StickNet Quality Control

All instrument biases were calculated by sampling relatively quiescent conditions prior to and following each phase of VORTEX2, in addition to several times throughout the project as field operations permitted. During each mass test, probes were simultaneously deployed for approximately 30-45 minutes, after which data were averaged to calculate the biases. Any probes that exceeded the maximum bias thresholds established by Markowski (2002) were removed.

2.4 Radar data

Data from the Center for Severe Weather Research (CSWR) Doppler On Wheels 6 (DOW6) mobile radar were used in this study. DOW 6 operates at a frequency of 9.375 GHz with a beamwidth of .93 degrees and gate length of as low as 12 m. This resolution is ideal for storm-scale analysis of severe weather phenomena. DOW6 reflectivity data were used in conjunction with data collected by StickNet probes.

3. METHODOLOGY

a. Variable Calculations

Deficits of equivalent potential temperature (Θ_e) and virtual potential temperature (Θ_v) were calculated within the forward and rear flanks of each storm relative to an inflow base state. Virtual potential temperature was calculated without consideration for liquid water precipitation, which will introduce a known positive bias in the calculations. Equivalent potential temperature was calculated using the equation developed by Bolton (1980).

b. Time-to-Space Conversion

In order to adequately assess the two-dimensional structure of a storm with in-situ observations, time-to-space conversion techniques were used in this study. In this scheme, it was assumed that the storm was steady state for a short window of time as it passed over an array of StickNet probes. Because the storm was assumed to be steady state, the storm motion vector was used to convert each data point in time into a point in space. Although in reality there are many relevant storm scale features that are certainly not steady state, it can be assumed that the bulk thermodynamic structure of a storm will remain sufficiently constant during this short window of time.

Once the data points were converted in space, the data were interpolated across the polygon bounded by the start and end points of each deployment using a Barnes analysis scheme. The radius of influence used in this study was approximately twice the average spacing between observations during a given deployment.

Reflectivity data taken from the Center for Severe Weather Research Doppler On Wheels 6

was overlaid onto the time-to-space conversion analyses to provide a storm-relative frame of reference. These data were only available for the westernmost array and, as such, WSR-88D radar data from Cheyenne, WY were used for analyses of the easternmost array. The analyses were performed for ten-minute intervals centered on 22:20:45, 22:24:49, 22:29:59, 22:43:14, 22:47:48 and 22:52:23 UTC. These times were chosen due to the availability of radar data at times when the mesocyclone was closest to the array of StickNet probes.

4. OBSERVATIONS

On June 5th 2009, VORTEX2 teams began operations in Sterling, CO and targeted a regime of upslope low-level winds across western Nebraska and southeast Wyoming. By mid-afternoon, multiple updrafts initiated along the higher terrain of southeast Wyoming, near the town of Chugwater. By 21:00 UTC, a dominant right-moving supercell emerged from this group of updrafts, and was declared a target storm at 21:18 UTC.

StickNet teams deployed two arrays of probes on the target storm. The westernmost array was deployed in a north-to-south orientation along Highway 85 approximately four miles to the west of LaGrange, WY, and approximately centered near the intersection of Highways 85 and 151. The easternmost array was deployed primarily in a north-to-south direction along County Road 237 starting from Highway 151. Because County Road 237 does not extend northward beyond Highway 151, one probe was dropped along Highway 151 eastward from the intersection with County Road 237. The arrays were spaced approximately 9-11 km apart, and spacing between probes was somewhat irregular due to an erratic storm motion. At approximately 22:25 UTC the mesocyclone of the target storm passed through the westernmost array. At this time, the supercell exhibited high precipitation characteristics and a mature tornado was ongoing that passed within a few hundred yards to the south of probe 110. This probe was the southernmost of the fine scale array. Other probes in the array also collected data from within the both the forward flank and rear-flank downdraft.

In all analysis times, three distinct air masses were identified within the storm environment. These three regions corresponded with the forward-flank, rear-flank downdraft, and inflow of the supercell. At the time of mesocyclone crossing, time-to-space conversion analysis revealed a deficit of 5K (4K) in theta-e (theta-v) (Figs. 1, 2) within the rear-flank downdraft. At the same time, deficits of theta-e (theta-v) within the forward flank measured to be as much as 12K (7K) (Figs. 1, 2). These deficits are greater than what would be expected for a tornadic storm based on the results of Markowski et al. (2002) and Shabbott (2006). However, it is worth noting that the tornado dissipated at approximately 22:31 UTC, before reaching the second array of probes, and was visibly showing signs of “roping out” as it intersected the westernmost array. It is entirely possible that the relatively large deficits played some role in the dissipation of the tornado; however, due to the lack of data taken during the tornadogenesis phase and shortly thereafter, this conclusion cannot be asserted.

The forward flank air mass was separated from the rear flank downdraft by a tongue of warm inflow air that extended from east to west immediately to the north of the mesocyclone and tornado (Figs. 1, 2). Thermodynamic deficits in this region were much smaller than those observed within both the rear and forward flanks. A sharp gradient in both theta-e and theta-v was observed between the forward flank and both the inflow and rear-flank downdrafts, and this gradient was collocated with the forward flank reflectivity gradient along its eastward extent. The tornado remained positioned between the inflow and rear-flank downdraft air mass within a regime of 3K deficits in theta-e. Theta-v deficits increased slightly from 2 to 3K within the vicinity of the tornado between 22:20:45 and 22:29:59 UTC.

As the storm crossed the array, radar data revealed a double gust front structure within the rear-flank downdraft. At 22:20:45 UTC, the leading gust front was positioned approximately 3.5 km to the east of the tornado, while the secondary gust front was positioned approximately 1.5 km to the east of the tornado. There was not a strong thermodynamic reflection of the leading gust front at the surface; however, the position of the secondary gust front was collocated with a gradient in both theta-e and theta-v. Wind data from probes 110 and 104 also did not strongly reflect the presence of the leading gust front; however, probe 110 (104) measured an increase from 3 m s^{-1} to 18 m s^{-1} (3 to 18 m s^{-1}) upon the

passage of the secondary gust front at 22:21:47 (22:22:30) (Fig. 5). At approximately 22:26:10, probe 110 measured a peak of 22 m s^{-1}, likely in response to the nearby tornado.

Although the storm would continue for several hours as an isolated supercell, the tornado had fully dissipated and the storm was showing signs of weakening both on radar and visually as it crossed the second array at approximately 22:48:00. At this point, the remnant hook echo was becoming disorganized and reflectivity was decreasing. Despite changes in the storm characteristics, the thermodynamic deficits remained approximately unchanged from the values measured by the first array in both the forward flank and the rear flank. The rear flank downdraft exhibited 5K (4K) deficits of theta-e (theta-v), while the forward flank exhibited deficits of 11K (7K) (Figs. 3, 4). Once again, a tongue of relatively warm inflow air separated the relatively cold forward flank from the cool rear flank downdraft. It is noted that the majority of the forward flank passed to the north of the probes within the second array, and thus may not have been adequately sampled for a direct comparison to the first array.

The mesocyclone passed slightly to the south of probe 222, which was the northernmost probe within the fine scale array. Although the thermodynamic deficits remained approximately constant between the two arrays, theta-e and theta-v both decreased more gradually across the rear-flank gust front in the second array than in the first (Figs. 4, 5). In addition, peak wind speeds immediately following the passage of the rear flank gust front were approximately 2-5 m s^{-1} lower than those measured in the first array. Probes 224, 223 and 217 exhibited significant variability in the winds following the passage of the rear-flank gust front. Probes 222, 223 and 224 exhibited an initial wind surge at approximately 22:44:00 UTC, followed by a secondary maximum at approximately 22:49:00 UTC and a tertiary maximum at approximately 22:51:00 UTC (Figs. 6, 7, 8). In each instance, the tertiary maximum was the strongest of the three. Probe 217 exhibited an initial maximum near 22:45:30 UTC as well as a secondary maximum near 22:49:30 UTC (Fig. 9). Due to the absence of DOW data during this time frame and the insufficient resolution of the available WSR-88D data, it cannot be determined whether or not these surges represented a coherent multiple gust-front structure similar to the rear flank gust front observed earlier in the storm's life cycle.

5. CONCLUSIONS

On June 5th 2009 VORTEX2 teams intercepted a supercell and incipient long-track EF-2 tornado. Scientists from Texas Tech University deployed twenty-three StickNet probes, separated into two arrays, and obtained samples of the forward flank, rear flank and near-mesocyclone environment during the mature tornadic and post-tornadic phases of the storm. Time-to-space conversion analysis was performed over six ten-minute intervals per array to analyze the two dimensional thermodynamic structure of the storm. Traces were also used to further diagnose the characteristics of gradients, particularly along the rear-flank gust front. Several key conclusions can be made based on the observations described in this study:

- Deficits of 5K (4K) in theta-e (theta-v) were observed within the rear-flank downdraft, while deficits of 11-12K (7K) were observed within the forward flank,
- The storm was characterized by three distinct airmasses: cold forward flank, cool rear flank, and warm inflow. The inflow wrapped around the north side of the mesocyclone and separated the forward flank from the rear flank,
- A sharp gradient in theta-e and theta-v was collocated with the forward flank reflectivity gradient during the mature tornadic phase,
- The thermodynamic deficits in both the forward flank and rear flank remained nearly constant between the mature tornadic phase and the post-tornadic phase,
- The thermodynamic gradient across the rear-flank gust front decreased between the mature tornadic phase and the post-tornadic phase,
- The tornado was located along a gradient in theta-e (theta-v) within a regime of 3K

(2-3K) deficits as it crossed the first array and dissipated, and

- Considerable kinematic variability was observed within the rear flank downdraft, including the presence of secondary and tertiary wind surges within the RFD.

The deficits observed in this study are larger than expected for a long-track tornadic supercell based on the most recent observational studies. However, since the measurements were only taken during the latter third of the tornadic life cycle and following dissipation, it is also possible that the moderately steep deficits contributed to the dissipation of the tornado. This conclusion cannot be reached without measurements of the storm during the earlier phases of the tornadic lifecycle. Future work will include several other VORTEX2 cases sampled during various tornadic and non-tornadic phases in order to further clarify the role of baroclinity in the formation and maintenance of tornadoes. In addition, data taken by NSSL Mobile Mesonet instruments will also be incorporated into future analysis.

6. ACKNOWLEDGEMENTS

This research was funded by National Science Foundation grant AGS-0800542. The authors of this paper wish to thank Dr. Joshua Wurman and the Center for Severe Weather Research for providing mobile DOW6 radar data and the National Climatic Data Center for providing archived WSR-88D radar data. All of the images and plots for this paper were generated using Matlab software. The assistance of Patrick Skinner and Brian Hirth in developing a time-to-space conversion method was invaluable and is greatly appreciated. In addition, thanks to Anthony Reinhart for assisting with data quality control. Finally, none of this research would be possible without the hard work of volunteers from Texas Tech University and the University of Michigan who assisted in data collection during VORTEX2.

7. REFERENCES

Bolton, D., 1980: The computation of equivalent potential temperature. *Mon. Wea. Rev.*, **108**, 1046-1053.

Grzych, M.L., B.D. Lee, and C.A. Finley, 2007: Thermodynamic analysis of supercell rear-flank downdrafts from project ANSWERS. *Mon. Wea. Rev.*, **135**, 240-246.

Hirth, B.D., J.L. Schroeder, and C.C. Weiss, 2008: Surface analysis of rear-flank downdraft outflow in two tornadic supercells. *Mon. Wea. Rev.*, **136**, 2344-2363.

Koch, S.E., M. desJardins, and P.J. Kocin, 1983: An interactive Barnes objective map analysis scheme for use with satellite and conventional data. *J. Climate Appl. Meteor.*, **22**, 1487-1503.

Lemon, L.R., and C.A. Doswell III, 1979: Severe thunderstorm evolution and mesocyclone structure as related to tornadogenesis. *Mon. Wea. Rev.*, **107**, 1184-1197.

Markowski, P.M., J.M. Straka, and E.N. Rasmussen, 2002. Direct surface thermodynamic observations within the rear- flank downdrafts of nontornadic and tornadic supercells. *Mon. Wea. Rev.*, **130**, 1692- 1721.

Shabbott, C.J., and P.M. Markowski, 2006: Surface in situ observations within the outflow of forward-flank downdrafts of supercell thunderstorms. *Mon. Wea. Rev.*, **134**, 1422-1441.

Skinner, P. and C.C. Weiss, 2008: Observations of storm scale boundary evolution within the 23 May 2007 Perryton, TX supercell. *Preprints, 24th Conference on Severe Local Storms*, Savannah, GA, *Amer. Meteor. Soc.*, P4.3 [Available online at http://ams.confex.com/ams/24SLS/techprogram/paper_141818.htm]

Weiss, C.C. and J.L. Schroeder, 2008: StickNet - A new portable, rapidly-deployable, surface observation system. *Preprints, 24th Conf. on IIPS*, New Orleans, LA, *Amer. Meteor. Soc.*, P4A.1 [Available online at http://ams.confex.com/ams/pdfpapers/134 04 7.pdf.]

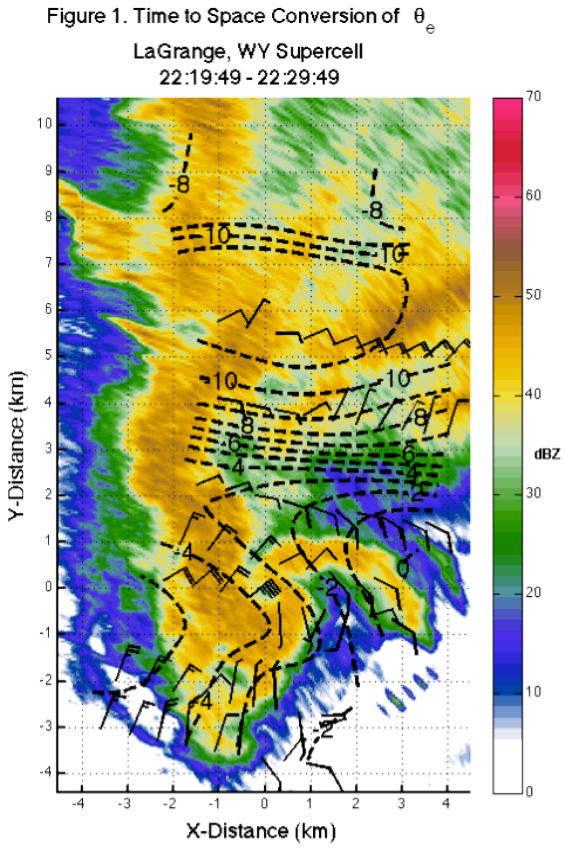

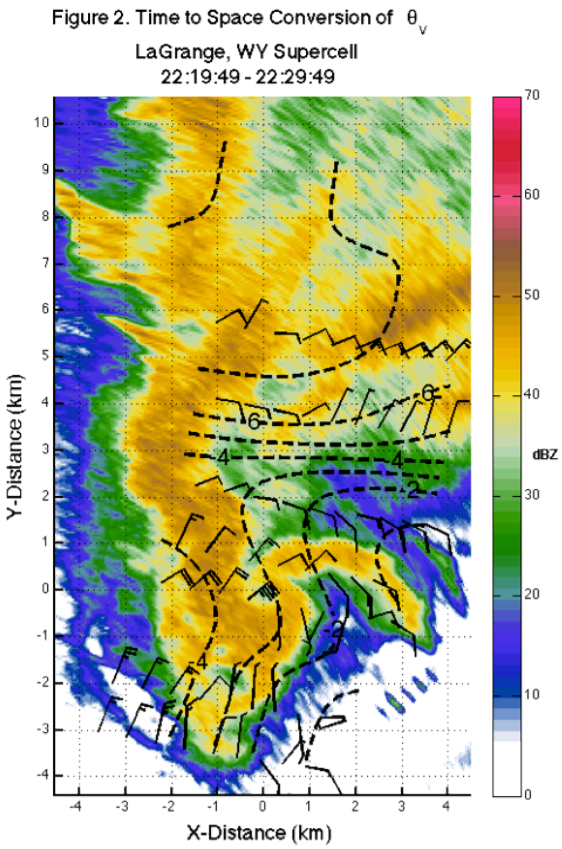

Figure 1 and 2: Objectively analyzed data of (1) equivalent potential temperature (K) and (2) virtual potential temperature (K) deficits (dashed contours) and time-to-space converted wind data (kts) overlaid on DOW6 reflectivity data at 22:24:49 UTC.

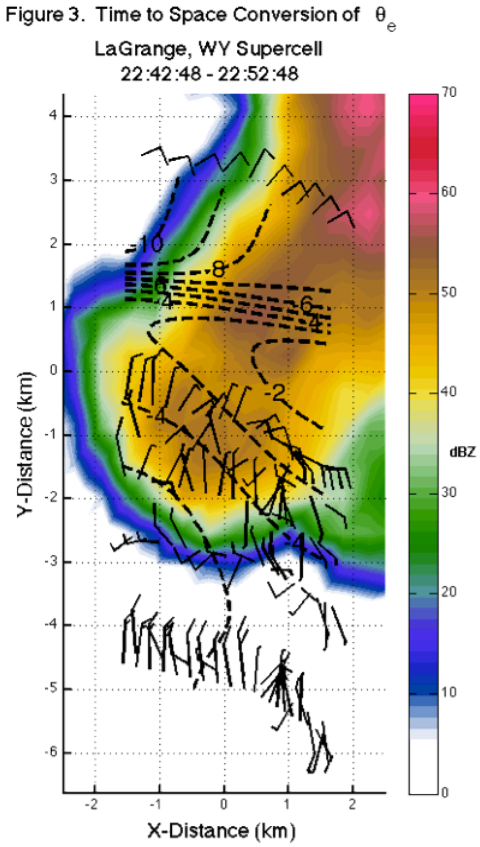

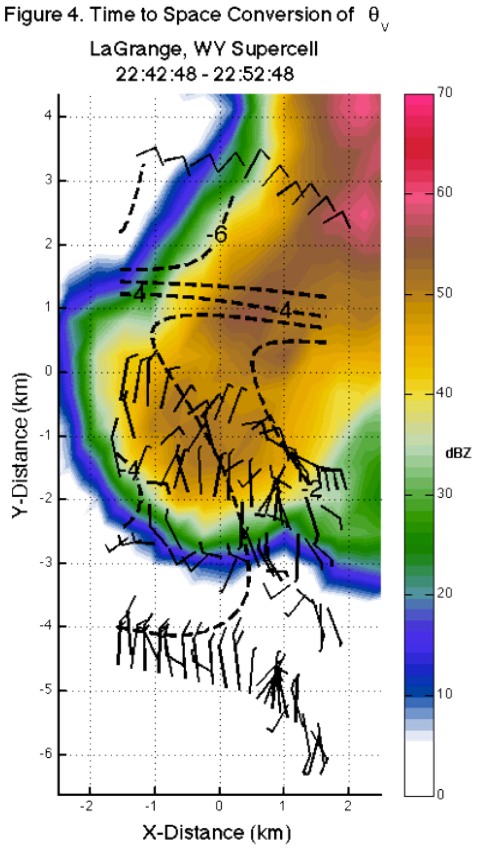

Figure 3 and 4: Objectively analyzed data of (1) equivalent potential temperature (K) and (2) virtual potential temperature (K) deficits (dashed contours) and time-to-space converted wind data (kts) overlaid on WSR-88D reflectivity data at 22:43:14 UTC.

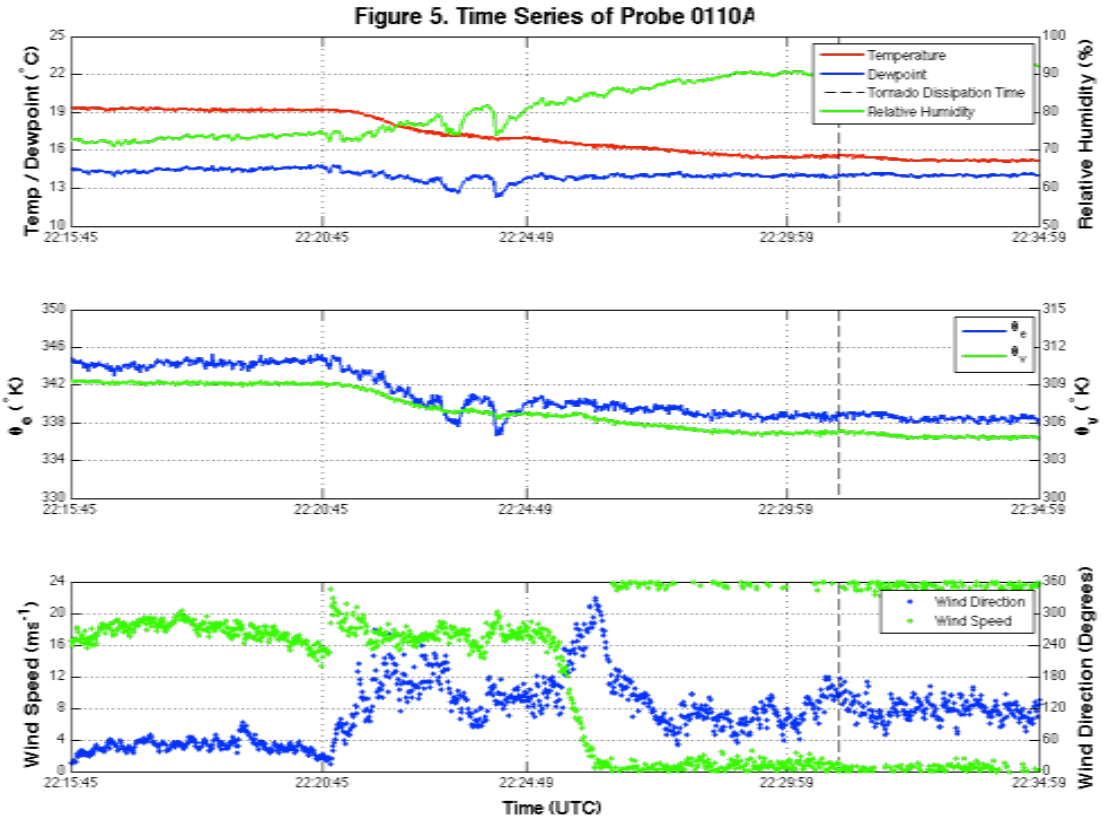

Figure 5: Time series of (top) temperature (red line), dewpoint (blue line), relative humidity (green line), (middle) equivalent potential temperature (blue line), virtual potential temperature (green line), (bottom) wind speed (blue dots) and direction (green dots) measured by probe 110A between 22:15:45 and 22:34:59 UTC. Vertical grid lines represent the times of DOW6 radar frames used in analysis, while the coarse dashed line represents the approximate time of tornado dissipation.

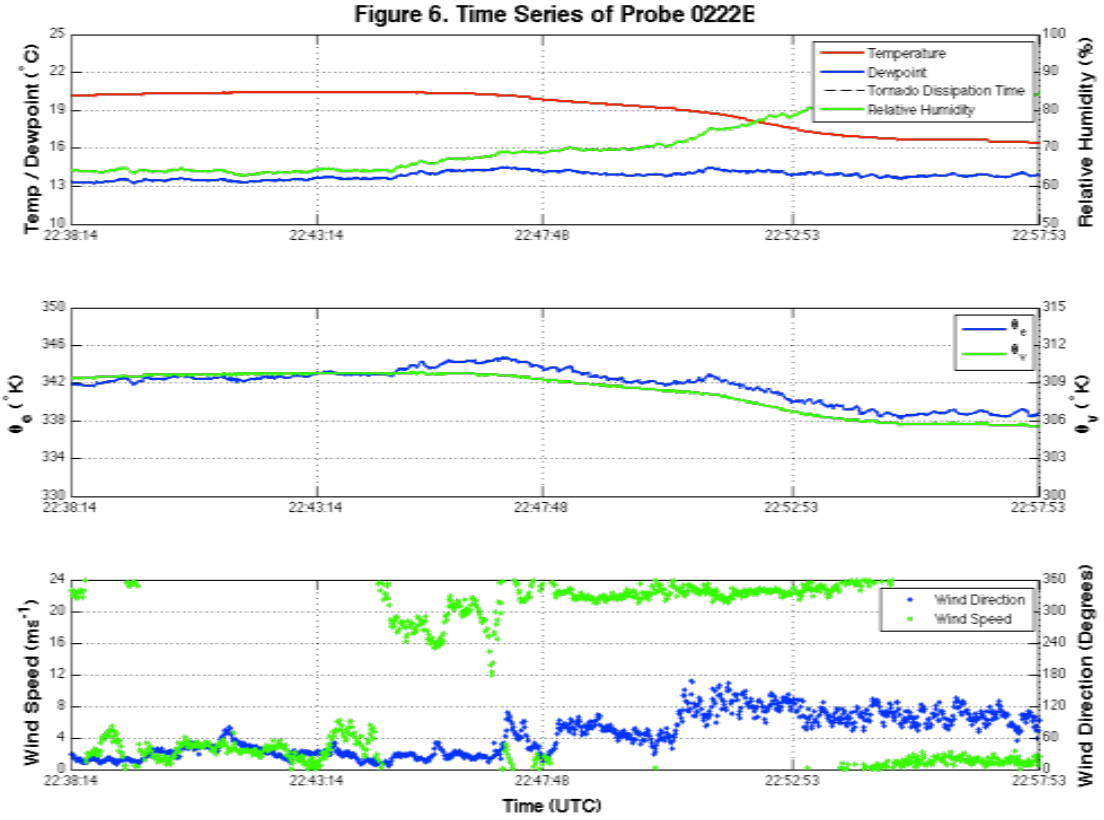

Figure 6: Same as Figure 5, but taken from probe 222B between 22:38:14 and 22:57:53 UTC. Dashed lines represent times of WSR-88D radar frames used in analysis.

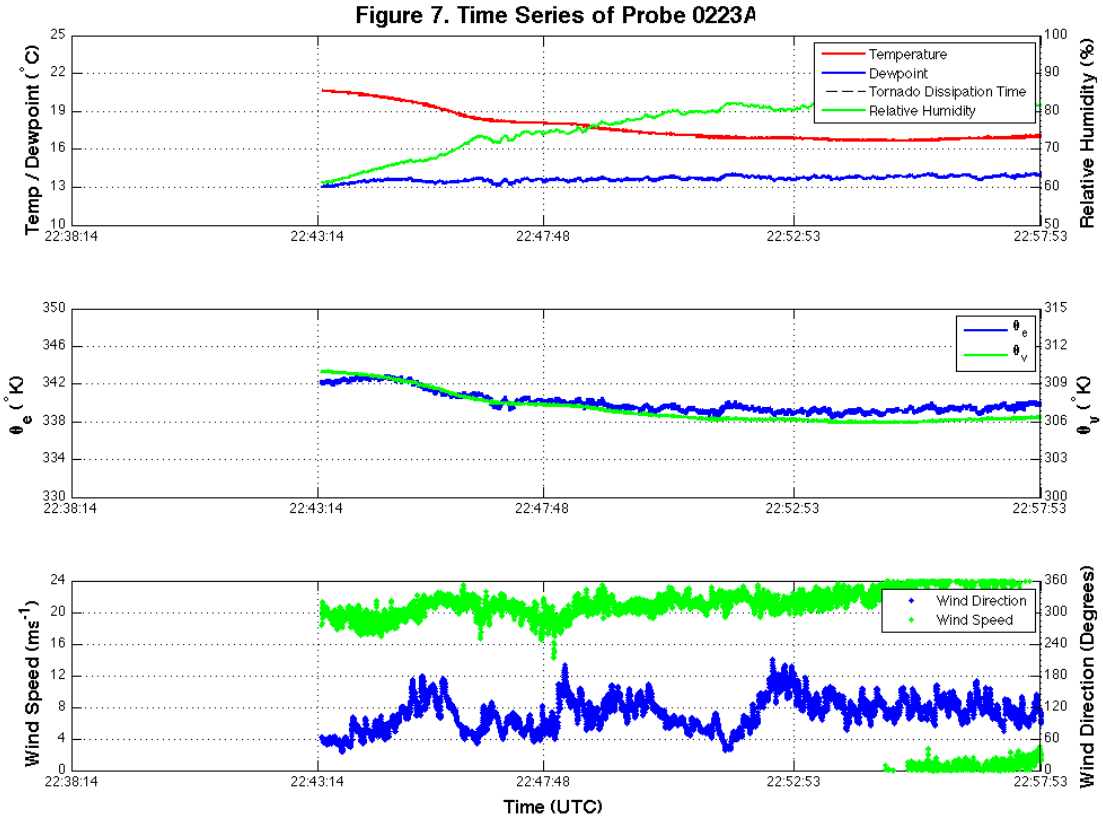

Figure 7: Same as Figure 6, but taken from probe 223A.

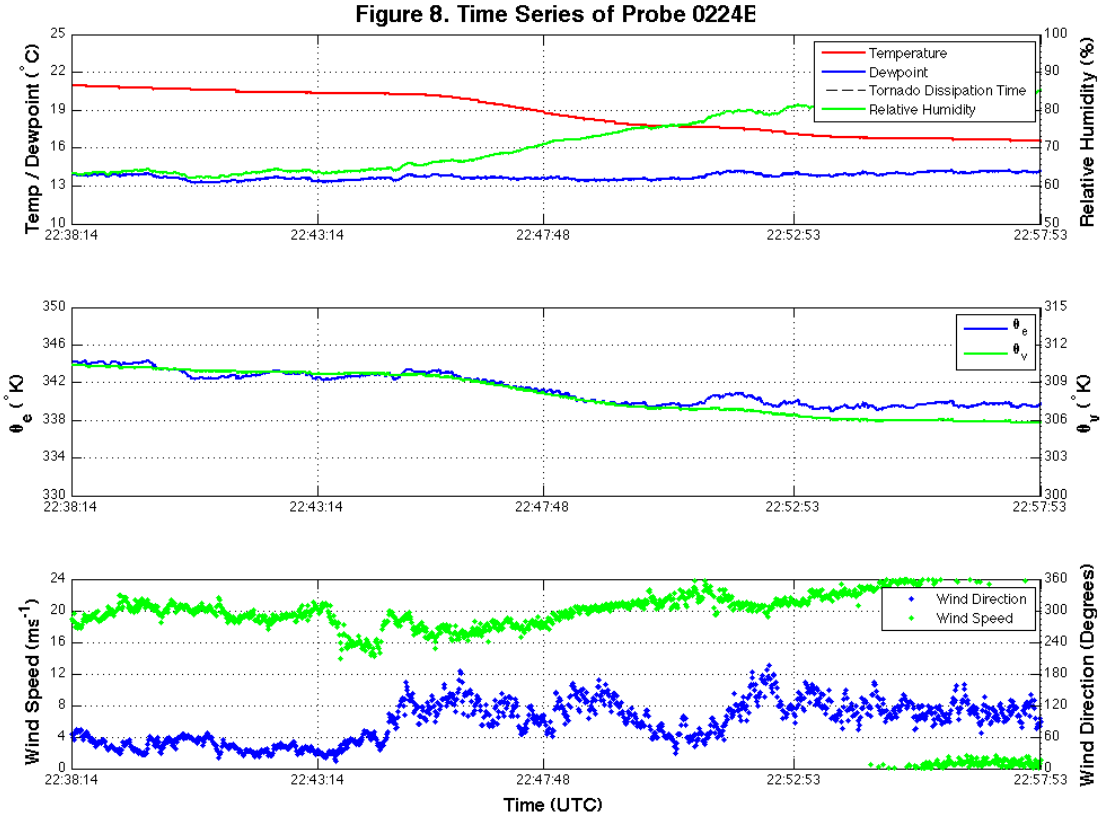

Figure 8: Same as Figure 7, but taken from probe 224B.

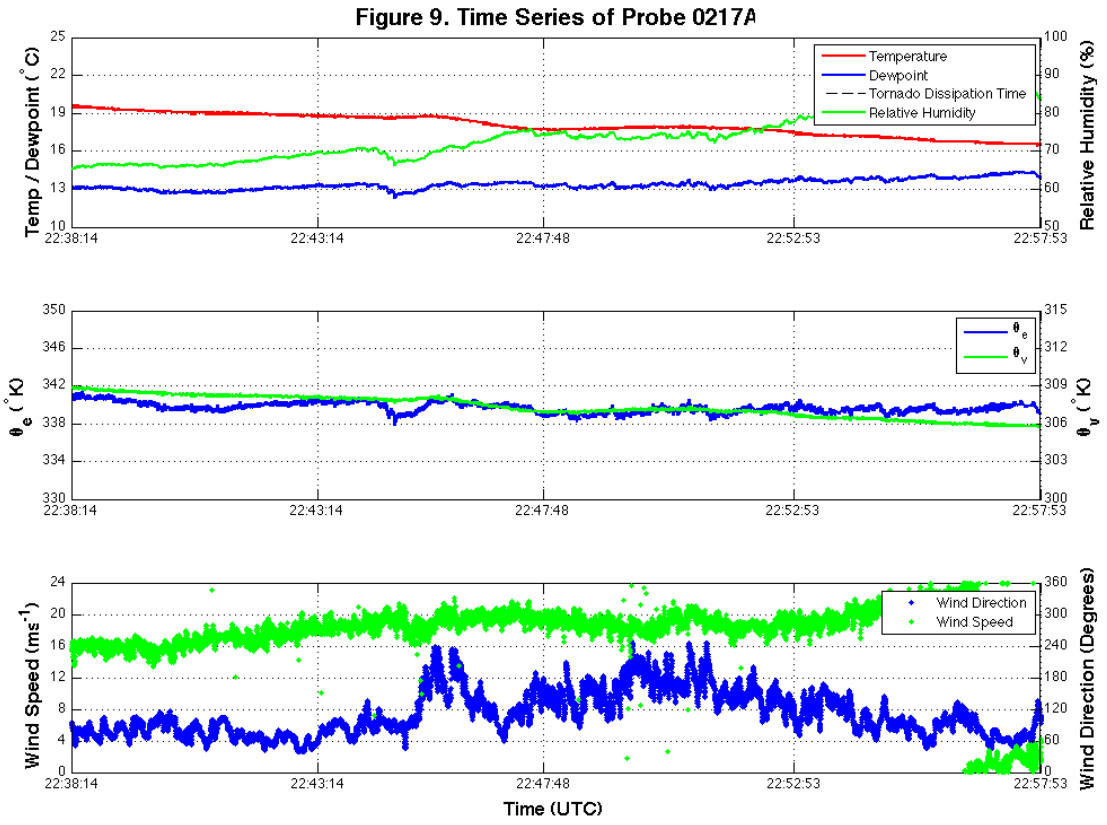

Figure 9: Same as Figure 8, but taken from probe 217A.